molecular pharmaceutics

ARTICLE

pubs.acs.org/molecularpharmaceutics

Formation of Stable Hydrophilic C_{60} Nanoparticles by 2-Hydroxypropyl-β-cyclodextrin

Daisuke Iohara,[†] Fumitoshi Hirayama,[*,†] Kenjirou Higashi,[‡] Keiji Yamamoto,[‡] and Kaneto Uekama[*,†]

[†]Faculty of Pharmaceutical Sciences, Sojo University, 4-22-1 Ikeda, Kumamoto 860-0082, Japan

[‡]Graduate School of Pharmaceutical Sciences, Chiba University, 1-8-1 Inohana, Chuo-ku, Chiba, 260-8675, Japan

Supporting Information

ABSTRACT: A number of papers have reported that the large cavity of γ-CyD is favorable for inclusion of C_{60} and forms a 1:2 (C_{60}:γ-CyD) complex, whereas it is thought to be difficult for β-CyD to form a complex at the molecular level. This is because the cavity size of β-CyD (0.78 nm) is smaller than the van der Waals diameter of C_{60} (1.0 nm). In this paper, we will report on the formation of the stable C_{60} nanoparticles by the hydrophilic 2-hydroxypropyl-β-cyclodextrin (HP-β-CyD) layer through weak interaction on the surface of the nanoparticles. C_{60} was coground with β-CyD, γ-CyD or HP-β-CyD mainly in a 1:2 molar ratio by an automatic magnetic agitating mortar, the coground powders were dispersed in water, and the resulting solutions were filtered through a pore size of 0.8 μm filter. The γ-CyD and HP-β-CyD systems gave transparent colloidal solutions consisting of C_{60}/CyD nanoparticles with the size lower than 100 nm, with high yields (about 100%). The C_{60}/HP-β-CyD nanoparticles are physically stable, keeping a small size for more than 28 days, whereas the γ-CyD nanoparticles are readily aggregated to form large particles (>800 nm). Solid and liquid NMR spectroscopic studies including measurements of spin−lattice relaxation times indicated that C_{60} interacted with γ-CyD and HP-β-CyD in the solid and colloidal solutions. When compared with the γ-CyD nanoparticles, adsorption studies of a hydrophobic dye on the surface of C_{60}/CyD nanoparticles indicated that the surface of the HP-β-CyD nanoparticles is largely covered by HP-β-CyD molecules forming hydrophilic hydration layers. The present results suggest that HP-β-CyD is useful for the preparation of C_{60} nanoparticles and medical applications such as photodynamic therapy, in spite of having a cavity size smaller than that of γ-CyD.

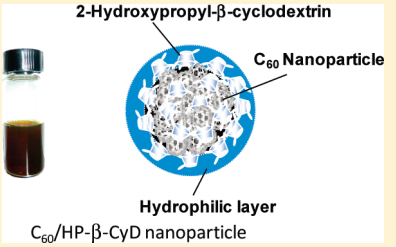

KEYWORDS: C_{60}, nanoparticle, aggregation, 2-hydroxypropyl-β-cyclodextrin, solid state NMR, surface property, adsorption

INTRODUCTION

Fullerenes are currently of great interest for practical applications that take advantage of their unique electronic properties and biological activities.[1] The fullerene family, especially C_{60}, has appealing photochemical, electrochemical and physical properties, which can be exploited in various medical fields.[2] For example, it can be used as a radical scavenger,[3] an antioxidant[4] and a carrier for gene[5] or drug[6] delivery systems. In addition, C_{60} has been regarded as an efficient photosensitizer for photodynamic therapy,[7,8] because of its light absorption property of relatively long wavelengths (S−S absorption, 530 nm, 920 nm; T−T absorption, 400 nm, 740 nm) and the high quantum yield of photoexcitation (1.0 based on generation of singlet oxygen).[9,10] In spite of the potential powerful photoinduced biological activities of C_{60}, its extremely low solubility in water has impeded further pharmaceutical applications.[11] Furthermore, even though solubilization has been achieved, it is well-known that fullerenes are easily aggregated, giving large particles or insoluble aggregates, depending on environmental conditions such as concentrations and solvent polarity.[12−14] Therefore, it is important to control the aggregation of C_{60}, because the aggregation significantly affects photophysical properties and biological activities.[15,16]

Several methods have been described for the preparation of water-soluble C_{60}, such as chemical modification of C_{60},[17,18] formation of water-soluble host−guest complexes[19,20] or solubilization by surfactants.[3,21] Among them, the solubilization using cyclodextrins (CyDs) is the most useful practical application of C_{60}, due to the good biocompatibility of CyDs. A number of papers[20,22] have reported that the large cavity of γ-CyD is favorable for inclusion with C_{60} and forms a 1:2 (C_{60}:γ-CyD) complex, whereas it is thought that it is difficult for β-CyD to form a complex at molecular dimensions. This is because the cavity size of β-CyD (0.78 nm) is smaller than the van der Waals diameter of C_{60} (1.0 nm). In spite of the smaller cavity of γ-CyD, we in a preliminary study[23] found that C_{60} forms stable colloidal solutions with 2-hydroxypropyl-β-cyclodextrin (HP-β-CyD). Furthermore, the C_{60}/HP-β-CyD nanoparticles had a high propensity for generating superoxide anions. The objective of this study was to elucidate the interaction of HP-β-CyD with C_{60} in water and consider the inhibiting mechanism of HP-β-CyD on the aggregation of C_{60}. We report here the formation of stable C_{60} nanoparticles by HP-β-CyD layer on the surface of C_{60} nanoparticles.

Received: February 8, 2011
Accepted: May 18, 2011
Published: May 18, 2011

EXPERIMENTAL SECTION

Materials. C_{60} (nanom purple SUH) was obtained from Frontier Carbon Co. (Tokyo, Japan). β-CyD, 2-hydroxypropyl-β-CyD (HP-β-CD, degree of substitution (D.S.) of 2-hydroxypropyl group was 5.6) and γ-CyD were donated by Nihon Shokuhin Kako Co., Ltd. (Tokyo, Japan). All other materials and solvents were of analytical reagent grade, and Milli-Q water was used throughout the study.

Preparation of Hydrophilic C_{60} Nanoparticles. C_{60} (15 mg) was ground with β-CyD (47 mg), γ-CyD (54 mg) or HP-β-CyD (60 mg) in different molar ratios (generally 1:2 for guest:host), using an automatic magnetic agitating mortar (MNV-01, AS ONE, Tokyo, Japan) for 3 h at 4 °C under reduced pressure. The pulverized C_{60}/CyDs were dispersed in water by ultrasonication for 5 min, to give about 1 mM of C_{60}, which was convenient for the size measurement of the nanoparticles by means of the dynamic light-scattering method described latter. The resulting solutions were syringe-filtered through a filter of 0.8 μm pore size. Concentrations of C_{60} in the colloidal solutions were determined by referring to the method of Deguchi et al.,[24] i.e. the C_{60} colloidal solution (1 mL) was mixed with 10% NaCl solution (1 mL) and heated at 80 °C for 1 h. After heating, 2 mL of toluene was added and then the mixture was sonicated for 10 min and centrifuged for 5 min at 4000 rpm to separate the water and toluene phases. The organic phase was carefully withdrawn, and the absorbance at 334 nm was measured. C_{60} powders were evaluated by powder X-ray diffractometry (Rigaku Ultima$^+$, Tokyo, Japan) under the following conditions: Ni-filtered Cu Kα radiation (1.542 Å), 40 kV, 40 mA, divergent slit of 1.74 mm (1°), scanning slit of 0.94 mm (1°), receiving slit of 0.15 mm, and goniometer angular increment of 2°/min.

Particle Size Analysis of C_{60}/CyD Nanoparticles. Particle sizes of the C_{60}/CyD colloidal solutions were determined by a dynamic light scattering machine (DLS-8000HL, Otsuka Electronics Co., Ltd. Tokyo, Japan) equipped with He−Ne laser (10 mW) operating at 632.8 nm. DLS measurements were performed at a scattering angle of 90°. The autocorrelation function was analyzed by the cumulant method to obtain the average particle diameter. Aggregation behavior of the C_{60}/CyD nanoparticles in water was studied at 25 °C in the dark. Zeta potentials for the colloids were determined using a Zetasizer (Nanozs, Sysmex Co., Tokyo, Japan). Transmission electron microscopy (TEM) images were taken on a FE-TEM (Philips TECNAI F20S-TWIN, Tokyo, Japan) operating at 200 kV. Specimens for TEM observations were prepared by putting the 150 mesh copper glid coated with a carbon film into the sample solution (C_{60} = 0.05 μM) and air-dried in the dark.

NMR measurements. All ^{13}C solid state NMR spectra were acquired using a JNM-ECA600 NMR spectrometer (JEOL Ltd., Tokyo, Japan) with a magnetic field of 14.09 T operating at 150 MHz for ^{13}C. Sample powders (ca. 100 mg) were placed into 4 mm silicon nitride (Si_3N_4) rotors. Spectra were acquired with the magic angle spinning (MAS) at 15 kHz and high-power two-pulse phase-modulation ^1H decoupling. Pertinent acquisition parameters included relaxation delays of 60 s for ^{13}C MAS NMR experiments. Variable amplitude cross-polarization (CP) was used for ^{13}C CP/MAS experiments setting up 5 ms contact time. All spectra were externally referenced to tetramethylsilane by setting the methyl signal of hexamethylbenzene to 17.2 ppm. Spin−lattice relaxation times (T_1^C) of ^{13}C in the coground C_{60}/CyD and CyD powders were measured with the CP T_1 pulse sequence (Torchia)[25] and T_1^C of C_{60} alone was measured with the inversion−recovery technique using pulse sequence $\pi-\tau-\pi/2$ at 25 °C.[26] ^{13}C NMR spectra were taken on a JNM-ECA500 Delta (11.75T) spectrometer (JEOL Ltd.) at 25 ∘C, using a 5 mm sample tube. C_{60}/HP-β-CyD and /γ-CyD coground powders were dispersed into D_2O to give 5 mg/mL of C_{60} concentration for NMR measurement.

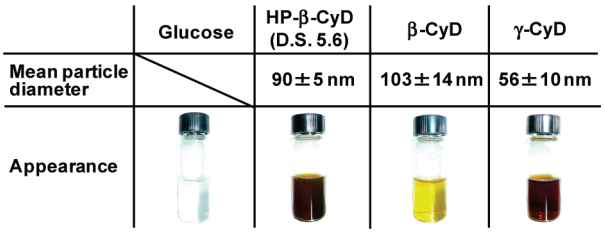

Figure 1. Mean particle diameter and appearance of the C_{60}/CyD and C_{60}/glucose colloidal solutions.

Hydrophobicity of C_{60}/CyD nanoparticles. Hydrophobicity of nanoparticle surfaces was evaluated by the binding affinity of Rose Bengal, a typical hydrophobic dye, on surface of the nanoparticles.[27] C_{60}/CyD nanoparticles (C_{60} = 70 μM) were incubated with different concentrations of Rose Bengal for 2 h at room temperature. The samples were centrifuged at 41000 rpm by ultracentrifuge for 1 h to spin down the particles. UV absorbance of supernatant at 548 nm was measured to determine the unbound Rose Bengal. The binding constant and the maximum amount bound were calculated from Scatchard plots according to the equation:[28]

$$r/a = K \cdot N - K \cdot r$$

where r is the amount of Rose Bengal adsorbed per mg nanoparticles (μg/mg); a is equilibrium concentration of Rose Bengal (μg/mL); K is the binding constant (mL/μg); and N is the maximum amount bound (μg/mg).

RESULTS AND DISCUSSION

Preparation of C_{60}/HP-β-CyD nanoparticles. C_{60} were coground with HP-β-CyD, β-CyD and γ-CyD in a molar ratio of 1:2 (C_{60}/CyD) and glucose in a molar ratio of 1:14 (C_{60}/glucose), by using the magnetic agitating mortar described in the experimental section. The resulting powders were dispersed in water and the suspensions were filtered through a filter of 0.8 μm pore. Figure 1 shows the appearances of the filtrates and the mean particle diameters of particles in the filtrates. When the C_{60}/glucose coground powders were dispersed in water, transparent solutions with no color were obtained, indicating that C_{60} existed in large aggregated states and the particles were completely filtered off by the 0.8 μm filter. On the other hand, transparent dark brown colored solutions were obtained when the C_{60}/HP-β-CyD or C_{60}/γ-CyD coground powders were dispersed in water. The C_{60}/parent β-CyD coground powder gave yellow colored solutions. This indicates large amounts of C_{60} were trapped on the filter with 0.8 μm pore size in the case of β-CyD. Figure 2 shows effects of the cogrinding time (Figures 2(a) and (b)) and molar ratio (Figures 2(c) and (d)) of C_{60}/CyD powders on the mean size of particles and the amounts (i.e., yield) of C_{60} particles in the filtrates. The mean diameter of the particles decreased when cogrinding time increased (Figure 2(a)) and the CyD/C_{60} molar ratio (Figure 2(c)), and

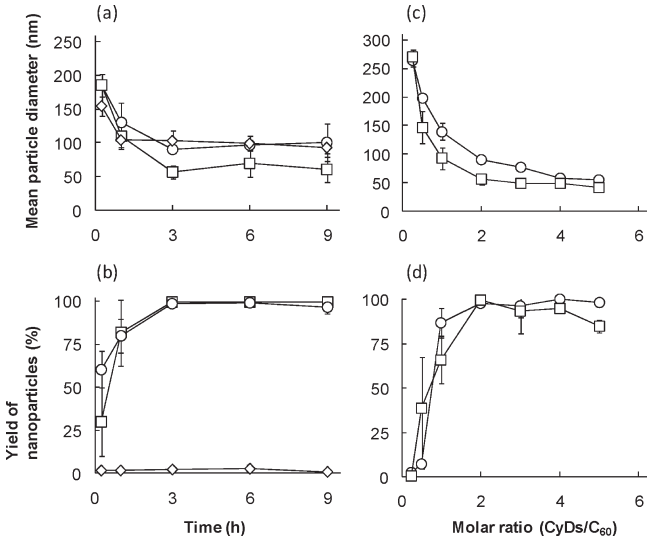

Figure 2. Effects of grinding time and C_{60}/CyD molar ratio on particle size (a, c) and yield (b, d) of C_{60} nanoparticles prepared using automatic magnetic agate mortar at 4 °C and reduced pressure. Each point represents the mean ± SE of 3−6 experiments. ○: C_{60}/HP-β-CyD colloidal solution. ◇: C_{60}/β-CyD colloidal solution. □: C_{60}/γ-CyD colloidal solution.

leveled off after the 3 h cogrinding and at a molar ratio of 2:1, reaching 103, 90, and 56 nm of the diameters for the β-CyD, HP-β-CyD and γ-CyD systems, respectively. In the case of HP-β-CyD and γ-CyD, C_{60} was quantitatively recovered in the filtrate (i.e., 100% yield) above the 3 h cogrinding (Figure 2(b)) and 2:1 molar ratio (Figure 2(d)), indicating that it changed to small sized particles and passed completely through the 0.8 μm filter. On the other hand, the parent β-CyD system gave the yield of 3% after the 3 h cogrinding (Figure 2(b)), suggesting almost all C_{60} existed as large particles and did not pass through the filter. We also conducted the filtration using 0.22 μm filters, and the same distribution of particle sizes was observed for these C_{60}/CyD systems. These results suggest that C_{60} is dispersed as nanoparticles, and the cogrinding method using HP-β-CyD and γ-CyD is useful in obtaining hydrophilic C_{60} nanoparticles with high yields.[29] The coground powders were therefore prepared in a molar ratio of 1:2 (C_{60}/CyD) and the grinding time was 3 h in the following study.

Aggregation Behavior of C_{60}/HP-β-CyD Nanoparticles. Figure 3 shows changes in the size of the nanoparticles in C_{60}/HP-β-CyD and C_{60}/γ-CyD colloidal solutions during storage at 25 °C in the dark. The initial size of the C_{60}/γ-CyD nanoparticle (55 nm) significantly increased with time and reached about 800 nm after 28 days, accompanying precipitation of dark colored powders of C_{60} including γ-CyD. In sharp contrast, the aggregation of C_{60}/HP-β-CyD nanoparticles was significantly inhibited, maintaining the small size for 28 days. The initial ζ-potentials of C_{60}/HP-β-CyD or γ-CyD nanoparticles in colloidal solutions were −19.7 and −20.8 mV respectively. The ζ-potential of C_{60} alone with 380 nm mean particle diameter was measured for a sample consisting of pristine C_{60} in water ultrasonicated for 1 h at 60 °C, then cooled down to room temperature and filtrated through a 0.8 μm filter. The ζ-potential of C_{60} alone was −28.2 mV. This ζ-potential was negatively larger than those of C_{60}/γ-CyD and HP-β-CyD nanoparticles, indicating that HP-β-CyD and γ-CyD shielded the negative

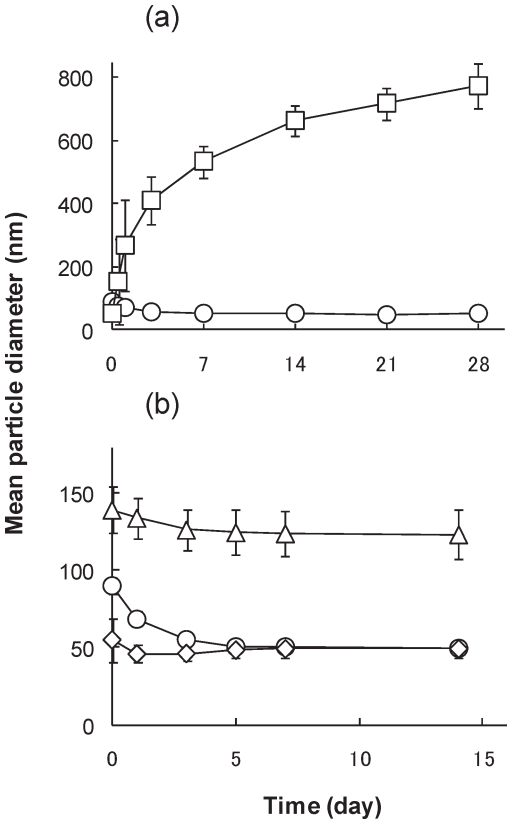

Figure 3. Changes in particle size of C_{60}/HP-β-CyD and C_{60}/γ-CyD colloidal solutions (a) and effect of HP-β-CyD concentrations on the C_{60} aggregation (b) as a function of storage time. Each point represents the mean ± SE of 3−6 experiments. ○: C_{60}/HP-β-CyD (1:2) colloidal solution. □: C_{60}/γ-CyD (1:2) colloidal solution. △: C_{60}/HP-β-CyD (1:1) colloidal solution. ◇: C_{60}/HP-β-CyD (1:5) colloidal solution.

charge of C_{60}, probably by means of interacting with the surface of the nanoparticles.[30] However, the negative ζ-potentials of the C_{60}/CyD colloidal solutions hardly changed during the storage, in spite of the different aggregations (Figure S1 in the Supporting Information). Therefore, it was difficult to explain the aggregation behavior of C_{60}/CyD colloidal solutions merely from a viewpoint of the change in ζ-potential. Figure 3b shows aggregation behavior of C_{60}/HP-β-CyD nanoparticles in different HP-β-CyD concentrations. When the ground C_{60}/HP-β-CyD (molar ratio = 1:1) powder was dissolved in water, the initial particle size of 140 nm slightly decreased to 120 nm with storage time, while it decreased to about 50 nm in the case of the molar ratio of the 1:2 system. The C_{60}/HP-β-CyD (molar ratio = 1:5) system maintained the initial small particle size, suggesting the high resistance to the aggregation at higher HP-β-CyD concentration. This resistance was suppressed by the addition of an inclusion competitor, i.e. the particle size of C_{60}/HP-β-CyD nanoparticles increased in the presence of ethyl *p*-hydroxybenzoate (Figure S2 in the Supporting Information). These results suggest that the interaction of HP-β-CyD plays an important role in the stabilization of C_{60} nanoparticles. Figure 4 shows TEM images of C_{60}/HP-β-CyD and C_{60}/γ-CyD nanoparticles in the colloidal solutions just after the dispersion. These images revealed that C_{60}/HP-β-CyD nanoparticles existed in fairly uniform spheres with 50 nm mean diameter and each particle was not seriously aggregated. C_{60}/γ-CyD nanoparticles existed in small spheres

with similar or rather smaller diameter, but the small particles are aggregated, probably because the aggregation took place in the drying process of TEM experiments.[14,24] Furthermore, the TEM images indicate that the aggregation of C_{60} nanoparticles is much more restricted in the HP-β-CyD system than in the γ-CyD system.

Interaction of C_{60} with CyDs in the Solid State. To gain insight into the inhibiting mechanism of HP-β-CyD on the C_{60} aggregation, the interaction of C_{60} and HP-β-CyD in the co-ground powders was studied by powder X-ray diffractometry and solid state NMR spectrometry. Figure 5 shows powder X-ray diffractograms of C_{60} powders ground with HP-β-CyD and γ-CyD in a molar ratio of 1:2 (C_{60}/CyD) and glucose in a molar ratio of 1:14 (C_{60}/glucose). Crystalline C_{60} gave diffraction peaks at 10.8°, 17.7° and 20.7°, and no change in these characteristic peaks was observed after the 3 h grinding (date not shown). In the case of the C_{60} powder coground with HP-β-CyD (Figure 5a), these sharp peaks markedly decreased when the grinding time was increased, and changed to broad peaks or halo-patterns when ground for more than 3 h. The C_{60} powder coground with γ-CyD gave a diffraction pattern similar to that of C_{60}/HP-β-CyD powders, although the broadening of the C_{60} peaks was smaller than that of the HP-β-CyD powder. The peak broadening is probably due to the interaction with CyDs. On the other hand, no change in the diffraction pattern was observed in the C_{60}/glucose system even after the 9 h grinding, indicating that both components were in crystalline states and negligibly interacted with each other. These results suggest that C_{60} exists as amorphous or finely dispersed small particles with low crystallinity in CyD powder matrices.

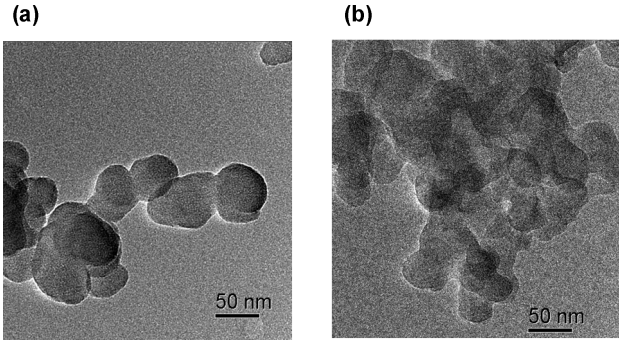

Figure 4. TEM images of C_{60}/HP-β-CyD (a) or C_{60}/γ-CyD (b) nanoparticles.

In the ^{13}C CP/MAS NMR spectra (Figure 6), coground C_{60}/HP-β-CyD and C_{60}/γ-CyD powders gave a sharp peak at 142.9 ppm assigned to C_{60} carbon, and relatively broad peaks at 60−100 ppm assigned to carbons of the CyD skeleton and the 2-hydroxypropyl moiety. It should be noted that the coground C_{60}/HP-β-CyD and C_{60}/γ-CyD powders gave the C_{60} carbon peak, whereas the physical mixture of both components gave no peaks of C_{60}. In the case of the C_{60}/glucose system, both the coground and simple mixtures gave no or negligible peaks. Under the cross-polarization (CP) conditions of the NMR measurements, the magnetization of the abundant spin system, ^{1}H nuclei, is efficiently transferred to the rare spin system, ^{13}C nuclei, which are in close contact with the ^{1}H nuclei through ^{13}C−^{1}H dipole−dipole interaction, thus enhancing the corresponding ^{13}C signal intensity. These ^{13}C CP/MAS NMR results suggest that C_{60} is in close contact with HP-β-CyD and γ-CyD protons in the coground powders, whereas there are no or negligible interactions in the physical mixtures and the C_{60}/glucose system.

Figure 7 shows ^{13}C MAS NMR spectra of coground C_{60}/CyD and ground C_{60} powders, acquired under no CP conditions. The ground C_{60} gave a peak at 143.0 ppm. On the other hand, the coground C_{60}/HP-β-CyD powder gave a peak at 143.0 ppm with the apparent shoulder peak and that of the C_{60}/γ-CyD powder gave two peaks at 143.0 ppm and 142.9 ppm. These results suggest that in the HP-β-CyD and γ-CyD matirices, C_{60} exists in

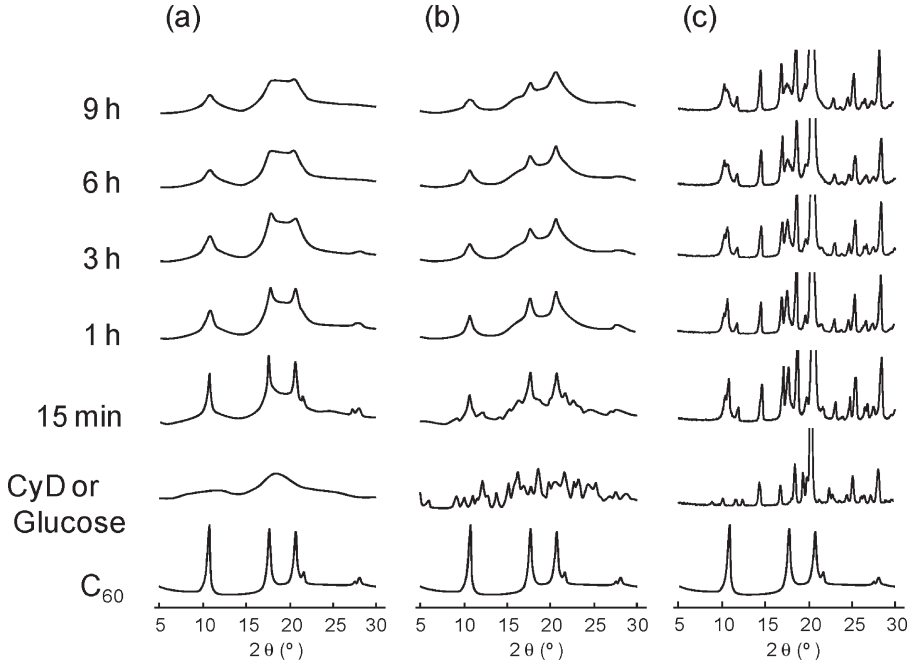

Figure 5. Powder X-ray diffraction patterns of C_{60} ground with HP-β-CyD (a), γ-CyD (b) or glucose (c) using automatic magnetic agate morter at 4 °C and reduced pressure.

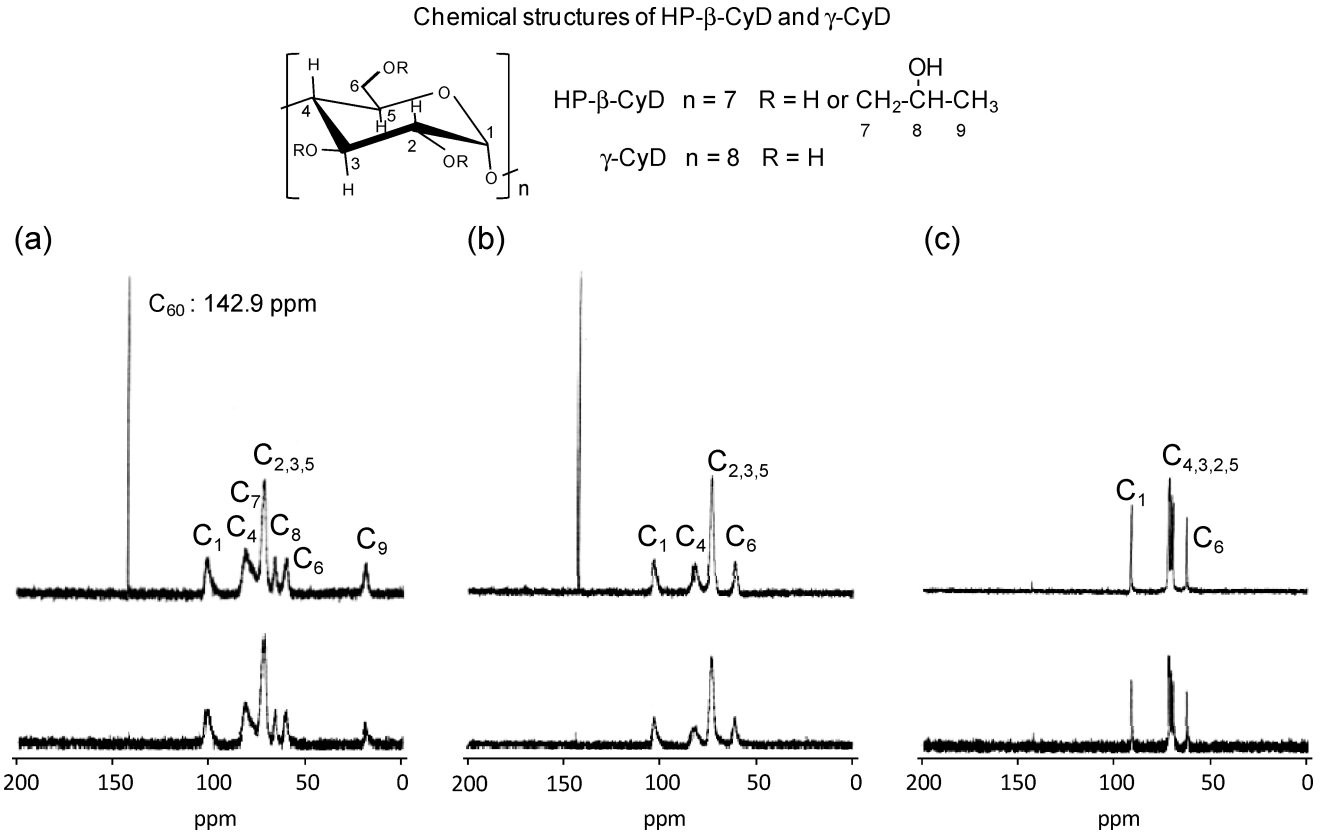

Figure 6. ^{13}C CP/MAS NMR spectra of C_{60} powder coground with HP-β-CyD (a), γ-CyD (b) or glucose (c) using automatic magnetic agate mortar. Upper: coground powder. Lower: physical mixture.

two magnetically different environments, whereas in the case of the ground C_{60}, it exists in only one state. In the ^{13}C CP/MAS spectra (Figures 6a,b) acquired under the CP condition, the single peak at 142.9 ppm is ascribable to the C_{60} carbon interacted with the CyDs. Therefore, we assigned the 143.0 ppm peak to the carbon of free C_{60} molecules and the 142.9 ppm peak to that of C_{60} molecules interacted with CyDs. It is well-known that C_{60} forms the inclusion complex with γ-CyD in a molar ratio of 1:2 (guest: host), in which the top and bottom of the guest are bicapped with the host.[20,22] These results suggest that the interaction of C_{60} with γ-CyD on the molecular level is stronger than that of HP-β-CyD, with the splitting of the peak in the former system greater than that in the latter system.

To gain further insight into the interaction between C_{60} and CyDs, T_1^C values of the carbons in the coground C_{60}/HP-β-CyD, C_{60}/γ-CyD, ground C_{60} and CyD powders were measured and are listed in Table 1. The T_1^C value (13.7 s) of the ground C_{60} carbon was markedly reduced to 4.4 s in the coground C_{60}/γ-CyD. The T_1^C values of the C1 (23.5 s), C4 (18.6 s) and C2,3,5 (14.3 s) of γ-CyD skeleton carbons were slightly lengthened in the coground C_{60}/γ-CyD, whereas that of the C6 carbon (1.4 s) in the primary hydroxyl group of CyD was shortened. It is reported that the motion of the rigid ring carbons of γ-CyD, i.e. C1, C4 and C2,3,5 carbons, is on the slow motional side of the T_1^C minimum because of its molecular size, whereas the C6 carbon of the primary hydroxyl group is on the fast motional side because of its fast internal rotation.[31] The molecular motion of C_{60} is reported to be in the narrowing region.[31] Taking these molecular motions into consideration, the reduction of the T_1^C of C_{60} observed in the coground C_{60}/γ-CyD suggests that the molecular motion of C_{60} is inhibited in the cavity, due to the inclusion complex formation. The increases in T_1^C values of the ring carbons and the decrease in that of the C6 carbon suggest that the motion of γ-CyD is slightly slowed down by the complex formation. On the other hand, the T_1^C (12.1 s) of C_{60} carbon in the coground HP-β-CyD was barely shorter than that of the ground C_{60} alone. The T_1^C of all HP-β-CyD carbons were almost the same as those of the ground HP-β-CyD alone, suggesting that HP-β-CyD only weakly interacts with C_{60}, and compared with γ-CyD, it does not completely include the guest into its cavity because of the small cavity size. Thus, the results of powder X-ray diffraction and solid state NMR studies suggest that the 1:2 inclusion complex[20,22] of C_{60}/γ-CyD coexists together with finely dispersed small C_{60} particles in γ-CyD powders, but HP-β-CyD may be adsorbed on the surface of dispersed small C_{60} particles, interacting weakly with C_{60}.

Interaction of C_{60} with CyDs in Colloidal Solutions. ^{13}C NMR studies in colloidal solutions were also carried out. As shown in Figure 8a, C_{60}/HP-β-CyD colloidal solutions gave the C_{60} peak at 145.5 ppm with a small shoulder peak, as seen in solid state NMR studies. This chemical shift agreed with the reported value for the C_{60} nanoparticles in D_2O.[32,33] On the other hand, the C_{60}/γ-CyD colloidal solution produced two peaks at 145.5 ppm with a small shoulder peak and at 145.3 ppm (Figure 8b). This indicated that C_{60}/γ-CyD nanoparticles probably consisted of three components of C_{60} in water, i.e. free C_{60} molecules, strongly and weakly interacting species with γ-CyD. Next, we measured the NMR spectra of supernatants after ultracentrifugation of C_{60}/HP-β- and γ-CyD colloidal solutions. Transparent solutions without any colors were obtained when the HP-β-CyD colloidal solutions

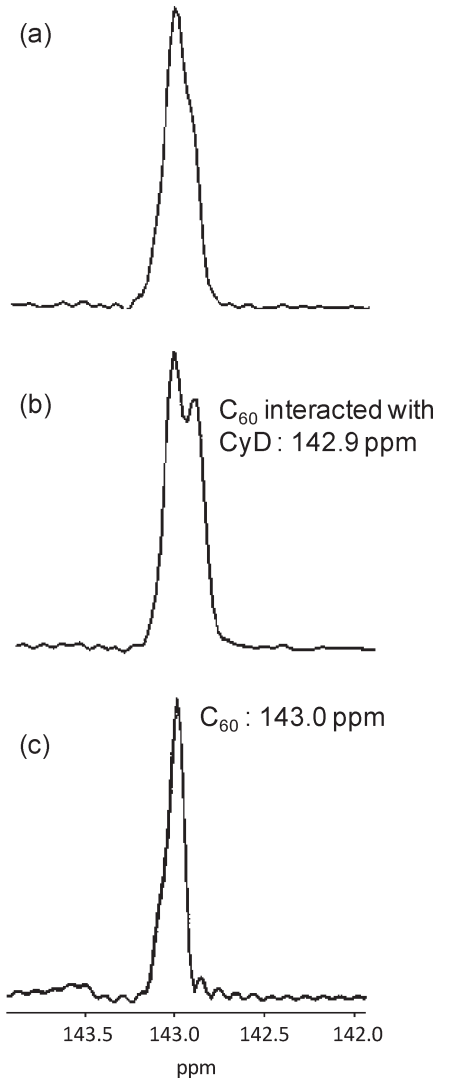

Figure 7. ^{13}C MAS NMR spectra of the C_{60} coground with HP-β-CyD (a) or γ-CyD (b) and ground C_{60} powder (c) using automatic magnetic agate mortar.

Table 1. T_1^C Values of Ground C_{60}/HP-β-CyD and C_{60}/γ-CyD evaluated from ^{13}C CP/MAS NMR Experiments (Torchia) at 25 °C[a]

	T_1^C (s)				
carbon	C_{60}	HP-β-CyD	C_{60}/HP-β-CyD	γ-CyD	C_{60}/γ-CyD
C_{60}	13.7		12.1		4.4
C_1		29.0	28.4	23.5	34.1
$C_{2,3,5}$		17.7	15.8	14.3	18.2
C_4		20.5	21.3	18.6	23.0
C_6		1.3	1.1	1.7	1.4
C_8		1.2	0.9		
C_9		0.7	0.7		

[a] The T_1^C value of the C7 carbon of HP-β-CyD never fit to the least-squares fitting due to the difficulty of determining the peak.

were ultracentrifuged, whereas transparent magenta colored solutions were obtained in the case of the γ-CyD colloidal solution. It is

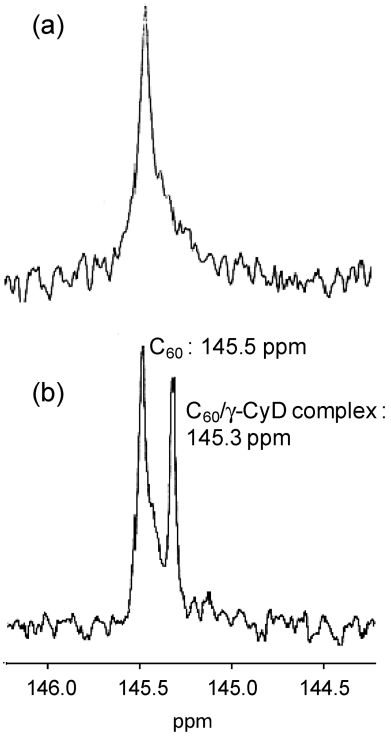

Figure 8. ^{13}C NMR spectra of C_{60}/HP-β-CyD (a) and C_{60}/γ-CyD (b) colloidal solutions at 25 °C.

reported that the transparent magenta solution consists of mainly the 1:2 complex of C_{60} and γ-CyD.[20,22] The $C_{60}(\gamma\text{-CyD})_2$ complex produced only one small single peak at 145.3 ppm (Figure S3 in the Supporting Information); this was the same as the peak observed in the C_{60}/γ-CyD colloidal solution. This data suggests that the peaks at 145.3 ppm observed in the NMR spectrum of C_{60}/γ-CyD colloidal solutions were certainly assigned to the C_{60}/γ-CyD inclusion complex. It is probable that the small shoulder peak seen in C_{60}/HP-β-CyD and C_{60}/γ-CyD colloidal solutions are assigned to the C_{60} molecules weakly interacting with CyD on surfaces of C_{60} nanoparticles. The proposed molecular state of C_{60} in the solid state and in water is shown in Scheme 1. When C_{60} is coground with CyDs, solid C_{60} is finely dispersed into CyD phases as nanoparticles. Once C_{60} nanoparticles and CyDs are dispersed in water, C_{60} maintains the nanostructure in water due to CyD layers and hydration[34] formed on the surface of C_{60} nanoparticles through the weak interaction or adsorption of CyDs. However, the deposition state of CyDs and hydration state may be different between the HP-β-CyD and γ-CyD nanoparticles, thus producing different aggregation behavior during the storage.

Adsorption behavior of a hydrophobic dye, Rose Bengal, on the nanoparticles was investigated to gain further insight into the surface properties of C_{60}/CyD nanoparticles. Because of the poor solubility and dispersibility of C_{60} in water, instead of pristine C_{60} (i.e., C_{60} alone), the C_{60}/β-CyD suspension without filtration was used as a control. Figure 9 shows adsorption volumes of Rose Bengal on the C_{60} nanoparticles. The volume adsorbed on C_{60}/HP-β-CyD nanoparticles showed the lowest value (ca. 20% of the loading volume) compared with others, and it increased in the order HP-β-CyD < γ-CyD < β-CyD nanoparticles. The UV spectroscopy confirmed that since the interaction of Rose Bengal with CyDs is negligible, the volume of the dye adsorbed on the nanoparticles can be a measure of

Scheme 1. Hydrophilic C_{60}/CyD Nanoparticles in the Solid State and in Water

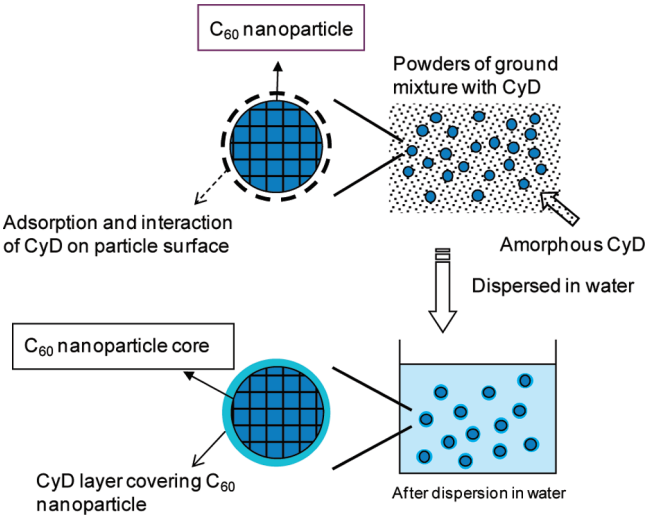

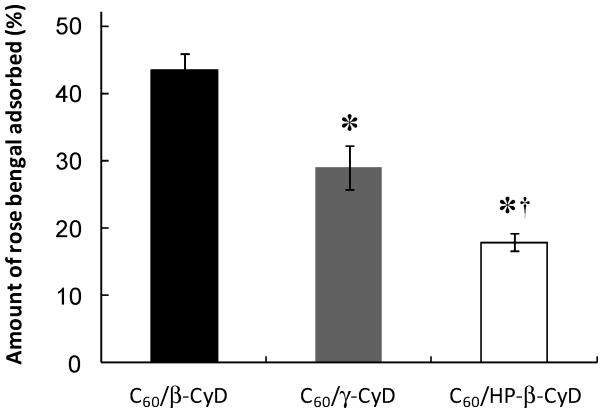

Figure 9. Amount of Rose Bengal adsorbed on surface of C_{60}/CyD nanoparticles. Each value represents the mean ± SE of 3 experiments. *, $p < 0.05$ versus C_{60}/β-CyD nanoparticles. †, $p < 0.05$ versus C_{60}/γ-CyD nanoparticles.

Table 2. Binding Constant (K) and Maximun Amount (N) of Rose Bengal Bound to the Surface of C_{60} Nanocrystals

C_{60} nanoparticles	K (mL/μg)	N (μg/mg)
C_{60}/HP-β-CyD	0.35	42
C_{60}/γ-CyD	0.28	66
C_{60}/β-CyD	3.13	80

hydrophobicity of the surface of the particles. Therefore, the adsorption results suggest that the surface of C_{60}/β-CyD suspensions is highly hydrophobic, whereas those of the γ-CyD and HP-β-CyD particles are rather hydrophilic. The binding parameters of Rose Bengal on the surface of nanoparticles calculated using Scatchard plots[28] (Figure S4 in the Supporting Information) are listed in Table 2. The C_{60}/β-CyD suspensions had high binding constant and maximum amount of Rose Bengal, compared with those of HP-β-CyD and γ-CyD nanoparticles. The maximum adsorbed amount of the dye on the HP-β-CyD nanoparticles was

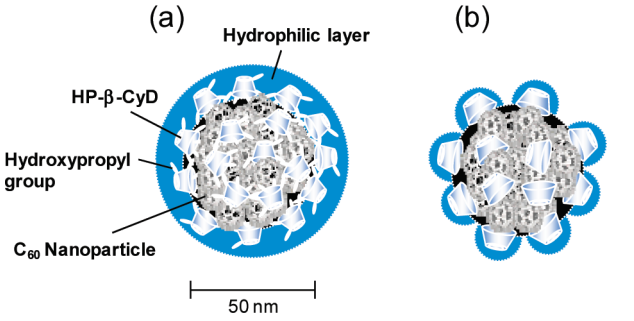

Figure 10. Proposed nanostructure of C_{60}/HP-β-CyD (a) and C_{60}/γ-CyD (b) nanoparticles.

smaller than that of the γ-CyD nanoparticles, while the values of the binding constants are almost the same (0.35 and 0.28 mL/μg respectively). This result suggests that C_{60}/HP-β-CyD nanoparticles have hydrophilic layers widely covered with HP-β-CyD, preventing the adsorption of the dye on the surface of C_{60} particles. The surface activity of CyDs is dependent on the hydrophobicity of substituents on the CyD ring.[35] Although the interaction strength is weak, because of its moderate surface activity (surface tensions of 2 mM γ-CyD and HP-β-CyD were 71 and 62 mN m^{-1}, respectively), the large coverage of C_{60} surfaces by HP-β-CyD may be attributable to hydrophobic interaction of the hydroxypropyl moieties of HP-β-CyD[36] with C_{60}.

We therefore proposed the structure of C_{60}/CyD nanoparticles, as shown in Figure 10. When the C_{60}/CyD coground powder is dispersed in water, C_{60} nanoparticles form uniform spheres covered with CyD layers. In the case of C_{60}/HP-β-CyD nanoparticles, HP-β-CyD widely covers the surface of C_{60} nanoparticles through the adsorption and interaction on/with the surface of C_{60}, as shown in Figure 10a, giving large hydration layers around the particles. In the case of the C_{60}/γ-CyD nanoparticle, the covered area is smaller than that of HP-β-CyD, as demonstrated by the Rose Bengal adsorption studies, shown in Figure 10b. This surface property of the γ-CyD nanoparticle leads to further aggregation during storage, whereas HP-β-CyD inhibits the aggregation. In addition, Loftsson et al. report that parent CyDs tend to self-assemble to form aggregates, while hydrophilic CyD derivatives have a lesser tendency to self-assemble in aqueous solutions.[37] For example, parent CyDs self-assemble to form a dimer, by facing the secondary hydroxyl sides of the molecules and by hydrogen-bonding each other.[38] This dimerization markedly lessens hydrations around the secondary hydroxyl sides of CyDs. γ-CyD is known to form the bicapped host dimer in which C_{60} is included. Therefore, the surface of the C_{60}/γ-CyD nanoparticle seems to be less hydrated, compared with that of the HP-β-CyD nanoparticle, when the 1:2 C_{60}/γ-CyD complexes are deposited on and around surface of the particle. This kind of property may also be responsible for the aggregation behavior of the C_{60} nanoparticles.

CONCLUSION

This paper has reported a simple procedure for the preparation of stable hydrophilic C_{60} nanoparticles by forming the HP-β-CyD layer. It is thought to be difficult for HP-β-CyD to form an inclusion complex with the C_{60} molecule, because of its smaller cavity compared with that of γ-CyD. However, our results revealed that C_{60} nanoparticles stably existed when HP-β-CyD coground powder was dispersed in water. Several

water-soluble fullerene derivatives were prepared, however, the chemical modification of C_{60} decreases its photophysical properties.[39,40] It can therefore be concluded that the solubilization of C_{60} without chemical modifications is a better approach in the pharmaceutical applications of C_{60}. Furthermore, the large aggregation of C_{60} significantly accelerates the decay of excited triplet state C_{60}, reducing its photosensitizing ability.[41] The present method is useful for the preparation of stable C_{60} nanoparticles and in the design of a drug delivery system for C_{60} in medicinal applications such as photodynamic therapy. We have confirmed that C_{60}/HP-β-CyD nanoparticles are prominent in the generation of reactive oxygen species, and this will be the focus for future research.

■ ASSOCIATED CONTENT

Supporting Information. Changes in ζ-potential as a function of storage time, effects of inclusion competitor on aggregation behavior of nanoparticles as a function of storage time, ^{13}C NMR spectrum of $C_{60}(\gamma\text{-CyD})_2$ complex, and Scatchard plots of Rose Bengal adsorbed on C_{60}/CyD nanoparticles. This material is available free of charge via the Internet at http://pubs.acs.org.

■ AUTHOR INFORMATION

Corresponding Author

*K.U. and F.H.: Faculty of Pharmaceutical Sciences, Sojo University, 4-22-1 Ikeda, Kumamoto 860-0082, Japan; Tel:+81-96-326-4096. Fax:+81-96-326-4096. E-mail: uekama@ph.sojo-u.ac.jp (K.U.) and fhira@ph.sojo-u.ac.jp (F.H.).

■ REFERENCES

(1) Jensen, A. W.; Wilson, S. R.; Schuster, D. I. Biological applications of fullerenes. *Bioorg. Med. Chem.* **1996**, *4*, 767–779.

(2) Bakry, R.; Vallant, R. M.; Najam-ul-Haq, M.; Rainer, M.; Szabo, Z.; Huck, C. W.; Bonn, G. K. Medicinal applications of fullerenes. *Int. J. Nanomed.* **2007**, *2*, 639–649.

(3) Xiao, L.; Takada, H.; Gan Xue, h.; Miwa, N. The water-soluble fullerene derivative "Radical Sponge" exerts cytoprotective action against UVA irradiation but not visible-light-catalyzed cytotoxicity in human skin keratinocytes. *Bioorg. Med. Chem. Lett.* **2006**, *16*, 1590–5.

(4) Dugan, L. L.; Turetsky, D. M.; Du, C.; Lobner, D.; Wheeler, M.; Almli, C. R.; Shen, C. K. F.; Luh, T.-Y.; Choi, D. W.; Lin, T.-S. Carboxyfullerenes as neuroprotective agents. *Proc. Natl. Acad. Sci. U.S.A.* **1997**, *94*, 9434–9439.

(5) Maeda-Mamiya, R.; Noiri, E.; Isobe, H.; Nakanishi, W.; Okamoto, K.; Doi, K.; Sugaya, T.; Izumi, T.; Homma, T.; Nakamura, E. In vivo gene delivery by cationic tetraamino fullerene. *Proc. Natl. Acad. Sci. U.S.A.* **2010**, *107*, 5339–5344.

(6) Zakharian, T. Y.; Seryshev, A.; Sitharaman, B.; Gilbert, B. E.; Knight, V.; Wilson, L. J. A Fullerene-paclitaxel chemotherapeutic: synthesis, characterization, and study of biological activity in tissue culture. *J. Am. Chem. Soc.* **2005**, *127*, 12508–12509.

(7) Liu, J.; Ohta, S.-I.; Sonoda, A.; Yamada, M.; Yamamoto, M.; Nitta, N.; Murata, K.; Tabata, Y. Preparation of PEG-conjugated fullerene containing Gd^{3+} ions for photodynamic therapy. *J. Controlled Release* **2007**, *117*, 104–110.

(8) Hamblin, M. R.; Mroz, P.; Tegos, G. P.; Gali, H.; Wharton, T.; Sarna, T.; Pawlak, A. Photodynamic therapy with fullerenes. *Fullerene Res. Adv.* **2007**, 1–31.

(9) Arbogast, J. W.; Darmanyan, A. P.; Foote, C. S.; Diederich, F. N.; Whetten, R. L.; Rubin, Y.; Alvarez, M. M.; Anz, S. J. Photophysical properties of sixty atom carbon molecule (C_{60}). *J. Phys. Chem.* **1991**, *95*, 11–12.

(10) Nagano, T.; Arakane, K.; Ryu, A.; Masunaga, T.; Shinmoto, K.; Mashiko, S.; Hirobe, M. Comparison of singlet oxygen production efficiency of C_{60} with other photosensitizers, based on 1268 nm emission. *Chem. Pharm. Bull* **1994**, *42*, 2291–4.

(11) Ruoff, R. S.; Tse, D. S.; Malhotra, R.; Lorents, D. C. Solubility of fullerene (C_{60}) in a variety of solvents. *J. Phys. Chem.* **1993**, *97*, 3379–3383.

(12) Nath, S.; Pal, H.; Palit, D. K.; Sapre, A. V.; Mittal, J. P. Aggregation of fullerene, C_{60}, in benzonitrile. *J. Phys. Chem. B* **1998**, *102*, 10158–10164.

(13) Alargova, R. G.; Deguchi, S.; Tsujii, K. Stable colloidal dispersions of fullerenes in polar organic solvents. *J. Am. Chem. Soc.* **2001**, *123*, 10460–10467.

(14) Brant, J. A.; Labille, J.; Bottero, J.-Y.; Wiesner, M. R. Characterizing the impact of preparation method on fullerene cluster structure and chemistry. *Langmuir* **2006**, *22*, 3878–3885.

(15) Mrzel, A.; Mertelj, A.; Omerzu, A.; Copic, M.; Mihailovic, D. Investigation of encapsulation and solvatochromism of fullerenes in binary solvent mixtures. *J. Phys. Chem. B* **1999**, *103*, 11256–11260.

(16) Fujitsuka, M.; Kasai, H.; Masuhara, A.; Okada, S.; Oikawa, H.; Nakanishi, H.; Watanabe, A.; Ito, O. Laser flash photolysis study on photochemical and photophysical properties of C_{60} fine particle. *Chem. Lett.* **1997**, 1211–1212.

(17) Friedman, S. H.; DeCamp, D. L.; Sijbesma, R. P.; Srdanov, G.; Wudl, F.; Kenyon, G. L. Inhibition of the HIV-1 protease by fullerene derivatives: model building studies and experimental verification. *J. Am. Chem. Soc.* **1993**, *115*, 6506–6509.

(18) Tokuyama, H.; Yamago, S.; Nakamura, E.; Shiraki, T.; Sugiura, Y. Photoinduced biochemical activity of fullerene carboxylic acid. *J. Am. Chem. Soc.* **1993**, *115*, 7918–7919.

(19) Ikeda, A.; Yoshimura, M.; Shinkai, S. Solution complexes formed from C_{60} and calixarenes. On the importance of the preorganized structure for cooperative interactions. *Tetrahedron Lett.* **1997**, *38*, 2107–2110.

(20) Yoshida, Z.; Takekuma, H.; Takekuma, S.; Matsubara, Y. Molecular recognition of C_{60} with γ-cyclodextrin. *Angew. Chem. Int. Ed. Engl.* **1994**, *33*, 1597–1599.

(21) Iwamoto, Y.; Yamakoshi, Y. A highly water-soluble C_{60}-NVP copolymer: a potential material for photodynamic therapy. *Chem. Commun.* **2006**, 4805–4807.

(22) Andersson, T.; Nilsson, K.; Sundahl, M.; Westman, G.; Wennerstroem, O. C_{60} embedded in γ-cyclodextrin: a water-soluble fullerene. *J. Chem. Soc., Chem. Commun.* **1992**, 604–606.

(23) Iohara, D.; Hirayama, F.; Kansui, H.; Aoshima, H.; Yamana, S.; Yano, M.; Kitaguchi, J.; Takashima, S.; Uekama, K. Preparation of hydrophilic nanoparticles of C_{60} with high resistance to aggregation during storage, using 2-hydroxypropyl-β-cyclodextrin. *Chem. Lett.* **2009**, *38*, 1104–1105.

(24) Deguchi, S.; Alargova, R. G.; Tsujii, K. Stable Dispersions of Fullerenes, C_{60} and C_{70}, in Water. Preparation and Characterization. *Langmuir* **2001**, *17*, 6013–6017.

(25) Torchia, D. A. The measurement of proton-enhanced carbon-13 T_1 values by a method which suppresses artifacts. *J. Magn. Reson.* **1978**, *30*, 613–616.

(26) Freeman, R.; Hill, H. D. W. Spin-lattice relaxation in high-resolution NMR spectra of carbon-13. *J. Chem. Phys.* **1970**, *53*, 4103–4105.

(27) Sahoo, S. K.; Panyam, J.; Prabha, S.; Labhasetwar, V. Residual polyvinyl alcohol associated with poly (D,L-lactide-co-glycolide) nanoparticles affects their physical properties and cellular uptake. *J. Controlled Release* **2002**, *82*, 105–114.

(28) Scatchard, G. The attraction of proteins for small molecules and ions. *Ann. N.Y. Acad. Sci.* **1949**, *51*, 660–672.

(29) Wongmekiat, A.; Tozuka, Y.; Oguchi, T.; Yamamoto, K. Formation of fine drug particle by cogrinding with cyclodextrins Part II. The influence of moisture condition during cogrinding process on fine particle formation. *Int. J. Pharm.* **2003**, *265*, 85–93.

(30) Pongpeerapat, A.; Wanawongthai, C.; Tozuka, Y.; Moribe, K.; Yamamoto, K. Formation mechanism of colloidal nanoparticles obtained from probucol/PVP/SDS ternary ground mixture. *Int. J. Pharm.* **2008**, *352*, 309–316.

(31) Tseng, W.-Y.; Chen, Y.-H.; Khairullin, I. I.; Cheng, S.; Hwang, L.-P. NMR study of solid C_{60}(γ-cyclodextrin)$_2$. *Solid State Nucl. Magn. Reson.* **1997**, *8*, 219–229.

(32) Deguchi, S.; Mukai, S.-A.; Yamazaki, T.; Tsudome, M.; Horikoshi, K. Nanoparticles of fullerene C_{60} from engineering of antiquity. *J. Phys. Chem. C* **2010**, *114*, 849–856.

(33) Fortner, J. D.; Lyon, D. Y.; Sayes, C. M.; Boyd, A. M.; Falkner, J. C.; Hotze, E. M.; Alemany, L. B.; Tao, Y. J.; Guo, W.; Ausman, K. D.; Colvin, V. L.; Hughes, J. B. C_{60} in water: nanocrystal formation and microbial response. *Environ. Sci. Technol.* **2005**, *39*, 4307–4316.

(34) Scharff, P.; Risch, K.; Carta-Abelmann, L.; Dmytruk, I. M.; Bilyi, M. M.; Golub, O. A.; Khavryuchenko, A. V.; Buzaneva, E. V.; Aksenov, V. L.; Avdeev, M. V.; Prylutskyy, Y. I.; Durov, S. S. Structure of C_{60} fullerene in water: spectroscopic data. *Carbon* **2004**, *42*, 1203–1206.

(35) Yoshida, A.; Arima, H.; Uekama, K.; Pitha, J. Pharmaceutical evaluation of hydroxyalkyl ethers of β-cyclodextrins. *Int. J. Pharm.* **1988**, *46*, 217–22.

(36) Uekama, K.; Hirayama, F.; Irie, T. Cyclodextrin drug carrier systems. *Chem. Rev.* **1998**, *98*, 2045–2076.

(37) Messner, M.; Kurkov, S. V.; Jansook, P.; Loftsson, T. Self-assembled cyclodextrin aggregates and nanoparticles. *Int. J. Pharm.* **2010**, *387*, 199–208.

(38) Gelb, R. I.; Schwartz, L. M.; Murray, C. T.; Laufer, D. A. Complexation of 4-biphenylcarboxylate by cyclohexaamylose. A conductometric and carbon-13 nuclear magnetic resonance spectrometric analysis. *J. Am. Chem. Soc.* **1978**, *100*, 3553–3559.

(39) Hamano, T.; Okuda, K.; Mashino, T.; Hirobe, M.; Arakane, K.; Ryu, A.; Mashiko, S.; Nagano, T. Singlet oxygen production from fullerene derivatives: effect of sequential functionalization of the fullerene core. *Chem. Commun.* **1997**, 21–22.

(40) Prat, F.; Stackow, R.; Bernstein, R.; Qian, W.; Rubin, Y.; Foote, C. S. Triplet-state properties and singlet oxygen generation in a homologous series of functionalized fullerene derivatives. *J. Phys. Chem. A* **1999**, *103*, 7230–7235.

(41) Lee, J.; Yamakoshi, Y.; Hughes, J. B.; Kim, J.-H. Mechanism of C_{60} photoreactivity in water: fate of triplet state and radical anion and production of reactive oxygen species. *Environ. Sci. Technol.* **2008**, *42*, 3459–3464.